Determination of Nonlinear Aerodynamic Coefficients Using the Estimation-Before-Modeling Method

Muthuthamby Sri-Jayantha*
IBM Research Division, Yorktown Heights, New York
and
Robert F. Stengel†
Princeton University, Princeton, New Jersey

Aerodynamic coefficients of a Schweizer 2-32 sailplane have been estimated from flight test data for angles of attack (α) up to 30 deg and sideslip angles (β) to ± 17 deg. The nonlinear aerodynamic model has been identified by applying the estimation-before-modeling (EBM) technique to flight data derived from 15 maneuvers including 7 stalls and "poststall gyrations." An extended Kalman-Bucy filter and a modified Bryson-Frazier smoother were used to estimate the time histories of the forces and moments from a 14 element discrete measurement vector. The optimal estimates and the measured control variables were sorted into 50 "subspaces," and the aerodynamic modeling was performed using a multiple regression scheme in each subspace. The linear and nonlinear portions of the coefficients could be observed from the modeling results, providing insight into the stall dynamic behavior of the sailplane. The accuracy of the aerodynamic coefficients was assessed by comparing measured time histories of the sailplane with a six-degree-of-freedom simulation model response. A novel aspect of the research is the use of a quaternion-based mathematical model of aircraft dynamics. A microprocessor-based data acquisition system was used onboard the sailplane.

Introduction

THE aerodynamic forces and moments acting on an aircraft at high angles of attack and sideslip are strongly nonlinear with respect to the aircraft state and control variables. The aircraft's dynamic behavior throughout its flight envelope is governed by the aerodynamic forces and moments, and the knowledge of the corresponding aerodynamic coefficients is of paramount importance in the analysis of the stall characteristics of the aircraft. The static, dynamic, and control coefficients that characterize the nondimensional aerodynamic coefficients of a full-scale aircraft must be estimated from flight testing data. Because full-scale wind-tunnel data are rarely available, efficient methods for collecting and processing flight data can benefit the development of new aircraft. In this research, the comprehensive nonlinear aerodynamic model of a Schweizer 2-32 sailplane has been obtained using the estimation-before-modeling (EBM) technique with flight data derived from 15 maneuvers that include stalls and "poststall gyrations." A novel aspect of the research is the use of a quaternion-based nonlinear mathematical model of aircraft attitude dynamics.

The EBM methodology consists of two distinct steps. In the first step, the time histories of the forces and moments corresponding to each maneuver are estimated using stochastic filtering and smoothing techniques. An extended Kalman-Bucy filter (EKF) and a modified Bryson-Frazier smoother are used for this purpose. In the second step, the optimal estimates along with the measured control variables that correspond to all 15 maneuvers are merged and sorted into several "subspaces." The modeling is performed in each subspace with a multiple regression scheme that used a partial F-test to select the statistically significant parameters.

The linear and nonlinear portions of the coefficients can be observed from the results. Static lift characteristics show gradual loss of lift beyond stall, while drag rises continuously with an increasing gradient. Pitch rate and elevator inputs contribute considerably to the total lift. A stable nose-down pitching moment is evident; the pitch damping and pitch control derivatives decrease with increasing angle of attack but remain effective into the poststall regime. The damping-in-roll and roll control derivatives become generally ineffective in the poststall regime. The accuracy of the aerodynamic coefficients is assessed by comparing the measured time histories of the sailplane with a six-degree-of-freedom simulation model response. A microprocessor-based data acquistion system was used on board and sailplane.[1,2] Details of the results and the experimental systems have been reported in Ref. 3.

System Identification Methodology

Estimation-Before-Modeling Technique

Aircraft parameter identification methodology has evolved from the use of static maneuvers through frequency testing to transient dynamic flight testing.[4] The maximum likelihood method is the most prevalent technique in aeronautics.[5] When the maximum likelihood method is used, the model structure of the unknown aerodynamic forces and moments must be specified in the parameter identification algorithm. If a different model structure is deemed necessary to accommodate specific maneuvers or aerodynamic assumptions, the algorithms must be reformulated. In the EBM technique, the state estimation and the aerodynamic model determination are carried out independently.[6] Accordingly, the aircraft's conventional state vector is expanded to include forces, moments, and selected sensor measurement calibration factors.

Aircraft Dynamic Model

The aircraft dynamic model contains six kinetic variables (u,v,w,p,q,r), five kinematic variables (e_1,e_2,e_3,e_4,z), six sets

Received March 23, 1987; revision received Sept. 28, 1987.

*Research Staff Member. T.J. Watson Research Center.
†Professor, Department of Mechanical and Aerospace Engineering. Associate Fellow AIAA.

of third-order Gauss-Markov parameters describing aerodynamic forces and moments, and nine sensor calibration components. These associated equations are collected into a general nonlinear vector differential form as follows:

$$\dot{x}(t) = f[x(t), u(t), w(t), t], x(0) = x_0 \quad (1)$$

where $x(t)$ is an n-dimensional state vector, [$\dot{}$] denotes the derivative with respect to time t, $u(t)$ is an m-dimensional control vector, and $w(t)$ is a disturbance input vector. The kinetic equations are defined as follows:

$$\begin{bmatrix} \dot{x}_1 \\ x_2 \\ x_3 \\ x_4 \\ x_5 \\ x_6 \end{bmatrix} = \begin{bmatrix} \dot{u} \\ v \\ w \\ p \\ q \\ r \end{bmatrix} = \begin{bmatrix} rv - qw + 2g(e_2e_4 - e_1e_3) + X \\ pw - ru + 2g(e_2e_3 + e_1e_4) + Y \\ qu - pv + g(e_1^2 + e_2^2 - e_3^2 - e_4^2) + Z \\ pqC_1 + qrC_2 + qC_3 + L + NC_4 \\ prC_5 + (r^2 - p^2)C_6 - rC_7 + M \\ pqC_8 + qrC_9 + qC_{10} + LC_{11} + N \end{bmatrix} \quad (2)$$

where u, v, and w (ft/s) are the axial, side, and normal velocity components, and p, q, and r (rad/s) are the roll, pitch, and yaw rates. Additional terms represent aerodynamic and inertial effects as follows:

$$X = qSC_X/m,\ Y = qSC_Y/m,\ Z = qSC_Z/m$$

$$L = qSb(C_\ell/I_{XX})[I_{XX}I_{ZZ}/(I_{XX}I_{ZZ} - I_{XZ}^2)]$$

$$M = qSc(C_m/I_{YY}) + [(Xm1_z - Zm1_x)/I_{YY}]$$

$$N = qSb(C_n/I_{ZZ})[I_{XX}I_{ZZ}/(I_{XX}I_{ZZ} - I_{XZ}^2)]$$

$$C_1 = [I_{XZ}(I_{ZZ} + I_{XX} - I_{YY})]/I^2$$

$$C_2 = [I_{ZZ}(I_{YY} - I_{ZZ}) - I_{XZ}^2]/I^2$$

$C_3 = 0$ (case with no rotating engine components)

$$C_4 = I_{XZ}/I_{XX}$$

$$C_5 = (I_{ZZ} - I_{XX})/I_{YY}$$

$$C_6 = I_{XZ}/I_{YY}$$

$$C_7 = 0$$

$$C_8 = [I_{XX}(I_{XX} - I_{YY}) + I_{XZ}^2]/I^2$$

$$C_9 = I_{XZ}(I_{YY} - I_{ZZ} - I_{XX})/I^2$$

$$C_{10} = 0$$

$$C_{11} = I_{XZ}/I_{ZZ}$$

$$q = (1/2)\rho V^2,\ I^2 = (I_{XX}I_{ZZ} - I_{XZ}^2)$$

The inertia matrix with elements $I_{(\cdot\cdot)}$ was obtained from full-scale oscillation tests, and it contains a nonzero off-diagonal term I_{XZ}. The aircraft mass (m) is located at a distance (ℓ_x, ℓ_z) from the aerodynamic center. V is the true airspeed, S is the reference area, b is the wing span, c is the mean aerodynamic chord, and ρ is the air density. The numerical values have been defined in Ref. 3. The remaining symbols, e_1 to e_4, are quaternions, which are defined below.

One of the problems associated with stall/spin research is that direct measurement of the aircraft's angular orientation may be constrained by mechanical limitations on attitude gyros. Using the rate-gyro outputs instead, the aircraft's attitude can be derived numerically. The widely used Euler angle representation contains a singularity at 90-deg pitch angle, preventing conventional algorithms from being used at large pitch angle. For singularity-free computation and improved numerical accuracy, representing vehicle attitude by quaternions has been found to be a better choice.[1] The quaternion components are progagated by the following kinematic equations:

$$\begin{bmatrix} \dot{x}_7 \\ x_8 \\ x_9 \\ x_{10} \end{bmatrix} = \begin{bmatrix} \dot{e}_1 \\ e_2 \\ e_3 \\ e_4 \end{bmatrix} = (1/2)\begin{bmatrix} 0 & -r & -q & -p \\ r & 0 & -p & q \\ q & p & 0 & -r \\ p & -q & r & 0 \end{bmatrix}\begin{bmatrix} e_1 \\ e_2 \\ e_3 \\ e_4 \end{bmatrix} \quad (3)$$

where e_1 to e_4 are the quaternion components. These equations are solved subject to an algebraic constraint:

$$e^Te = 1 \quad (4)$$

This normality condition is enforced by renormalizing the quaternions at the end of each filter and smoother update, as described later. The altitude (represented by $-z$, ft) then is propagated by

$$\dot{x}_{11} = \dot{z} = 2u(e_2e_4 - e_1e_3) + 2v(e_2e_3 + e_1e_4) + w(e_1^2 + e_2^2 - e_3^2 - e_4^2) \quad (5)$$

The specific aerodynamic forces and moments are modeled as third-order Gauss-Markov process. The problem of selecting a specific aerodynamic model structure for X, Y, Z, L, M, and N is circumvented by first estimating the total values of the aerodynamic forces and moments using the Gauss-Markov formulation. The model is described by

$$\dot{b} = [L]b \quad (6a)$$

where

$x_{12} = b_{10} = X$ = Axial specific force, ft/s^2

$x_{15} = b_{20} = Y$ = Side specific force, ft/s^2

$x_{18} = b_{30} = Z$ = Normal specific force, ft/s^2

$x_{21} = b_{40} = L$ = Roll specific moment, rad/s^2

$x_{24} = b_{50} = M$ = Pitch specific moment, rad/s^2

$x_{27} = b_{60} = N$ = Yaw specific moment, rad/s^2

The unlisted components (e.g., x_{13}, x_{14}, x_{16},...) are first and second derivatives of the specific forces and moments. The matrix L of Eq. (6a) is block diagonal with a block matrix defined, for example, by the following model:

$$\begin{bmatrix} \dot{x}_{12} \\ x_{13} \\ x_{14} \end{bmatrix} = \begin{bmatrix} 0 & 1 & 0 \\ 0 & 0 & 1 \\ 0 & 0 & 0 \end{bmatrix}\begin{bmatrix} x_{12} \\ x_{13} \\ x_{14} \end{bmatrix} + \begin{bmatrix} w_{12} \\ w_{13} \\ w_{14} \end{bmatrix} \quad (6b)$$

where $x_{12} = X$ (axial specific force) and w_i are Gaussian white noise processes. The third-order Gauss-Markov model provides a reasonable compromise between the total model order and the anticipated time-rates-of-change in forces. Equation (6b) yields a three-term quadratic interpolation polynomial as a function of time (where the three terms are updated by the filter at each sampling instant).

Sensor calibration constants represent the aerodynamic angle biases, aerodynamic angle scale factors, and rate gyro biases ($x_B = x_{30}$ to x_{38}). These quantities are modeled as random constants:

$$\dot{x}_B = 0 \quad (7)$$

The filter/smoother algorithm was tested by numerical simulation and with data derived from the flight tests of a single-engine Navion aircraft.[7] The algorithm was found to be nondivergent, and agreement between measured and estimated attitude angles was good.

Aircraft Measurement Model

The algebraic/transcendental equations of measurement can be written as,

$$z(t) = h[x(t),\ u(t),\ t] + v(t)$$

$$= y(t) + v(t) \tag{8}$$

In the experiment, the vector $z(t)$ contains 14 components. The four control-surface measurements are required in the modeling phase of EBM and are not required in the estimation phase. The mathematical model of $z(t)$ is as follows:

Three linear acceleration measurements (a_x, a_y, a_z):

$$\begin{bmatrix} z_1 \\ z_2 \\ z_3 \end{bmatrix} = \begin{bmatrix} a_x \\ a_y \\ a_z \end{bmatrix} \quad \begin{bmatrix} X - (r^2+q^2)x + (pq-r)y + (pr+q)z \\ Y - (p^2+r^2)y + (pq+r)x + (qr-p)z \\ Z - (p^2+q^2)z + (pr-q)x + (qr+p)y \end{bmatrix} \tag{9}$$

The accelerometers are clustered and located at (x, y, z), and the terms (X, Y, Z) represent the specific forces.

Three angular acceleration measurements ($\dot{p}_m$, $\dot{q}_m$, $\dot{r}_m$):

$$\begin{bmatrix} z_4 \\ z_5 \\ z_6 \end{bmatrix} = \begin{bmatrix} \dot{p}_m \\ \dot{q}_m \\ \dot{r}_m \end{bmatrix} = \begin{bmatrix} pqC_1 + qrC_2 + qC_3 + L + NC_4 \\ prC_5 + (r^2 - p^2)C_6 - rC_7 + M \\ pqC_8 + qrC_9 + qC_{10} + LC_{11} + N \end{bmatrix} \tag{10}$$

Three angular rate measurements (p_m, q_m, r_m):

$$\begin{bmatrix} z_7 \\ z_8 \\ z_9 \end{bmatrix} = \begin{bmatrix} p_m \\ q_m \\ r_m \end{bmatrix} = \begin{bmatrix} p \\ q \\ r \end{bmatrix} + \begin{bmatrix} b_p \\ b_q \\ b_r \end{bmatrix} \tag{11}$$

where the constants b_p, b_q, and b_r represent the instrument bias, and are modeled as random constants [Eq. (7)].

One total airspeed measurement (corrected for the pressure and temperature variation V_m):

$$z_{10} = V_m = (u_1^2 + v_1^2 + w_1^2)^{1/2} \tag{12}$$

where

$$\begin{bmatrix} u_1 \\ v_1 \\ w_1 \end{bmatrix} = \begin{bmatrix} u \\ v \\ w \end{bmatrix} + \begin{bmatrix} 0 & -r & q \\ r & 0 & -p \\ -q & p & 0 \end{bmatrix} \begin{bmatrix} x \\ y \\ z \end{bmatrix} \tag{13}$$

and (x, y, z) defines the location of the airdata probe.

Two angle-of-attack measurements (on right and left wings):

$$z_{11} = \alpha_{RW_m} = (1 + a_{\alpha_{RW}})\ \alpha_{RW} + b_{\alpha_{RW}} \tag{14}$$

where

$$\alpha_{RW} = \tan^{-1}(w_1/u_1) \tag{15}$$

One sideslip-angle measurement on the right wing (β_{RW_m}):

$$z_{13} = \beta_{RW_m} = (1 + a_{\beta_{RW}})\ \beta_{RW} + b_{\beta_{RW}} \tag{16}$$

where

$$\beta_{RW} = \tan^{-1}(v_1/u_1) \tag{17}$$

Note that the definition of the sideslip angle β_{RW} is not conventional; however, it can be transformed to the usual definition [$\beta = \sin^{-1}(v_1/V)$] quite readily. The subscripted variables a and b correspond to the measurement scale-factor and bias errors respectively, and are modeled as random constants [Eq. (7)].

One altitude measurement (H_m):

$$z_{14} = H_m = -z \tag{18}$$

Aircraft State Estimation

In principle, the parameter identification could be done without prior state estimation, other than to transform measured quantities to desired dependent and independent variables of interest. However, optimal state estimation preceding aerodynamic modeling provides a statistical basis for minimizing the effects of measurement error subject to the known dynamic constraints of the aircraft's physical model. The optimal state estimation is achieved using an extended Kalman-Bucy filter and a modified Bryson-Frazier smoother. Note that the dynamic model is continuous but the observation vector is discrete. The EKF is implemented as follows:[8]

Initial Condition

The initial state x_0 is computed using the trim data (i.e., steady-state flight) preceding each maneuver. The state covariance matrix P_0 is chosen to be a diagonal matrix with fixed elements for all maneuvers.

Process and Measurement Noise

The process matrix R and the measurement noise matrix Q are obtained through prior tuning and engineering judgment. It was found sufficient to tune the filter only once. Numerical values have been reported in Ref. 3.

State and Covariance Extrapolation

The numerical interpolation of the state and covariance from time $t_k(+)$ to $t_{k+1}(-)$ is performed using a double-precision (64-bit) fourth-order Runge-Kutta integration scheme, where the $(-/+)$ corresponds to the time instant just-before/immediately-after an update:

$$\dot{x}(t) = f[x(t)] \tag{19}$$

$$\dot{P}(t) = F(t)P(t) + P(t)F^T(t) + Q \tag{20}$$

where

$$F(t) = \left.\frac{\partial f}{\partial x}\right|_{x\ k(t)} \tag{21}$$

The equation (20) governing the state covariance dynamics is known as the matrix Riccati equation (continuous dynamics and discrete measurement).

The elements of $F(t)$ are obtained from the function $f[x(t)]$ by analytical differentiation. The quaternion normalization is obtained as shown in the following.

$$[e(+)]_{\text{normalized}} = \{1/[e(+)^T e(+)]^{1/2}\}\ e(+) \tag{22}$$

For *Kalman gain matrix*, the filter gain is as follows

$$K_k = P_k(-)H_k^T(-)\ [H_k(-)P_k(-)H_k^T + R_k]^{-1} \tag{23}$$

where

$$H_k = \left.\frac{\partial h}{\partial x}\right|_{x\ k(-)} \tag{24}$$

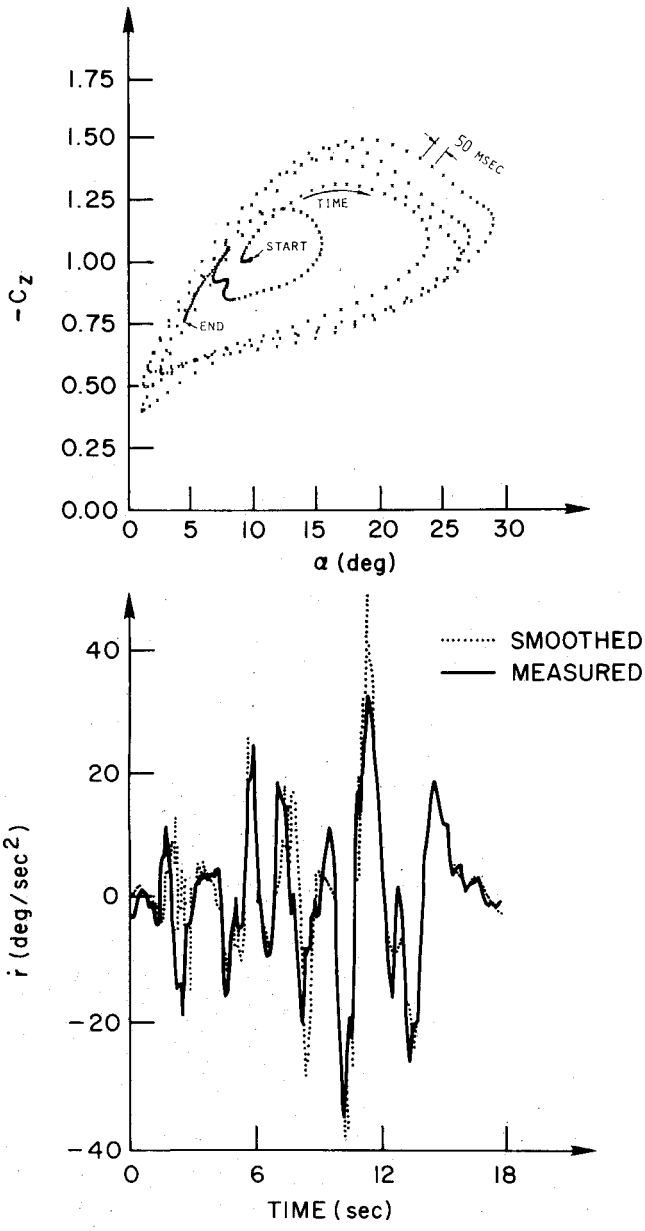

Fig. 1 a) Smoothed $(-C_Z)$ vs α, b) Measured/smoothed yaw acceleration $\dot{r}$.

The *state and covariance updates* are as follows:

$$x_k(+) = x_k(-) + K_k\{z_k - h[x_k(-)]\} \tag{25}$$

$$P_k(+) = \{I - K_k H_k[x_k(-)]\}\, P_k(-) \tag{26}$$

Using the intermediate results of the EKF and by introducing adjoint variables, the modified-Bryson-Frazier (MBF) smoother achieves improved estimates of the state. The adjoint variables are generated from a reverse time Kalman-like filter,[9] as summarized:

Initial condition of the adjoint variables λ and Λ are initialized according to

$$\lambda(T-) = -H_N{}^T D_N{}^{-1} \Delta z_N \tag{27}$$

$$\Lambda(T-) = H_N{}^T D_N{}^{-1} H_N \tag{28}$$

where

$$D_N = H_N(-) P_N H_N{}^T(-) + R_N \tag{29}$$

$$\Delta z_N = [z_N - h(x_N(-))] \tag{30}$$

Propagation of adjoint variables, is carried out through the numerical integration from $t_{k+1}(-)$ to $t_k(+)$, and is performed backward in time according to

$$\dot{\lambda} = -F^T \lambda \tag{31}$$

$$\dot{\Lambda} = -F^T \Lambda - \Lambda^T F \tag{32}$$

The *updates of the adjoint variables* at $t = t_k$ are obtained from

$$\lambda_k(-) = \lambda_k(+) - H_k{}^T D_k{}^{-1}[\Delta z_k + D_k K_k{}^T \lambda_k(+)] \tag{33}$$

$$\Lambda_k(-) = (I - K_k H_k)^T \Lambda_k(+)(I - K_k H_k) + (H_k{}^T D_k{}^{-1} H_k) \tag{34}$$

Note that the smoothed state and covariance estimates [as given by Eqs. (35) and (36)] are not included in the adjoint variable update.

The *smoothed estimates* of the state x and the covariance P are computed as follows:

$$[x_k(+)]_{\text{smooth}} = [x_k(+)]_{\text{filter}} - P_k(+)\lambda_k(+) \tag{35}$$

$$[P_k(+)]_{\text{smooth}} = [P_k(+)]_{\text{filter}} - P_k(+)\Lambda_k(+)P_k(t) \tag{36}$$

The quaternion components are normalized according to Eq. (22). The smoothed estimates are obtained by correcting the filter estimates, and no recursion is performed on the smoothed estimates.

Multivariate Regression for Aerodynamic Coefficient Modeling

Time histories of C_X, C_Y, C_Z, C_ℓ, C_m, C_n are derived from the smoothed estimates of X, Y, Z, L, M, and N with V computed from the smoothed estimates of (u, v, w) and air density ρ computed from the smoothed estimates of h. Denoting any one of the six aerodynamic coefficients by $y(t)$, the independent variables (such as angle of attack, angular rates, control inputs, etc.) by a vector $x(t)$, and the associated (yet unknown) parameters by θ, a general form for the aerodynamic model can be assumed as follows:

$$y(t) = \theta_0 + \theta_1 x_1(t) + .. + \theta_{n-1} x_{n-1}(t) + \epsilon(t) \tag{37}$$

Here, $\epsilon(t)$ represents the error due to estimation of $x(t)$ and θ. The general aerodynamic model represented by Eq. (37) is linear in x_1, x_2,..., but each of these elements can in general represent a linear or nonlinear combinations of the independent variables that may affect the aerodynamic coefficient. When N observations are available for $y(t)$ and $x(t)$, Eq. (37) can be put into a matrix form, and the least-square estimate of the parameter vector θ can be computed according to

$$\hat{\theta} = (X^T X)^{-1} X^T y \tag{38}$$

where $\hat{\theta}$, which is the estimate of θ, and is an $(n \times 1)$ vector of parameters; y is the $(N \times 1)$ vector of smoothed values, and X is the $(N \times n)$ matrix of smoothed independent variables.[10] The corvariance of the parameter estimates can be shown to be

$$\text{Var}(\hat{\theta}) = s^2 (X^T X)^{-1} \tag{39}$$

where

$$s^2 = \{\Sigma[\hat{y}(i) - y(i)]^2\}/(N - n) \tag{40}$$

$$\hat{y}(i) = \hat{\theta}_0 + \hat{\theta}_1 x_1(i) + .. + \hat{\theta}_{n-1} x_{n-1}(i) \quad (41)$$

Several criteria can be used to select the most significant set of parametervector coefficients.[11] The partial F-test was employed in this research to build up the parameter vector. The partial F-test method is discussed in Ref. 3. The coefficients that are linear in α and β are forced into the aerodynamic models regardless of their significance level. The matrix X^TX plays an important role in the performance of the regression algorithm. In order to estimate the parameters with finite variance, the information matrix $(X^TX)^{-1}$ must be nonsingular. In practice, a nonsingular information matrix is obtained by providing sufficient dynamic variation to the independent variables through appropriate input to the aircraft. Centering of data reduces the risk of illconditioning due to roundoff errors, where the mean value of each variable is removed from its total value before the computation of $(X^TX)^{-1}$. The problem of linear dependence with polynomial regression can be minimized by the choice of orthogonal polynomials[10] in the construction of X. For example, if α and α^2 are two chosen variables, the orthogonal polynomial set $(\alpha - \bar{\alpha})$ and $(\alpha - \bar{\alpha})^2$ is preferable to α and α^2 ($\bar{\alpha}$ denotes the mean value of the samples).

Experimental System

The Schweizer 2-32 sailplane was equipped with a microprocessor-based data acquisition system.[2] A 12-bit, 32-channel, analog-to-digital converter was used to digitize the sensor voltages conditioned by the presampling filters. Identical active second-order low-pass Bessel filters with 6.5 Hz cutoff frequency were used in all the data channels. (The Bessel filter has the best linear phase lag property for providing minimum signal distortion.) In order to minimize quantization error, the sensor outputs were biased and amplified to match the analog-to-digital converter input range. The data acquisition system was based on two Z-80 processors. The data digitized by the first processor at 20 samples/s was transferred to a second processor for on-board storage on a magnetic tape cartridge.[12] Under the pilot's command, the microprocessors could provide real-time display of sensor outputs either in engineering units or in raw digital format, facilitating onboard monitoring or calibration of the sailplane's sensors. About ten maneuvers were performed between each takeoff and landing of the sailplane each lasting for about 25 s. The recorded flight data was transferred to a general-purpose computer (IBM 3081) through an RS-232 link for EBM processing and validation.

Flight Testing and Estimation of Aerodynamic Coefficients

Flight Test Summary

Fifteen maneuvers were performed at low and high α, β conditions, including seven stalls and "poststall gyrations." For the first maneuver, the elevator was pumped to excite the short period mode of the sailplane. For the second maneuver, both aileron and rudder were pumped to excite the dutch roll mode. For the third maneuver, only the rudder was pumped. In the remaining maneuvers, the three controls were moved in a random fashion while driving the sailplane into a stall.

State Estimation

The 38 state elements of each maneuver were estimated using EKF and MBF algorithms. The estimation phase took more than 90% of the total computing time. The smoothed normal force coefficient (C_Z) vs α of a stall maneuver is shown in Fig. 1a. The figure shows not only the static component of C_Z as a function of α but also the dynamic contribution of pitch rate and other independent variables. The aircraft enters the stall from a trim α of 9 deg, goes through several cycles of pitch oscillation, and ultimately recovers and trims at an α of 4 deg. The markedly different values of C_Z for increasing and decreasing α are largely explained by the linear dynamic effects of q and $\dot{\alpha}$; they are not thought to represent "true" hysteresis, which would be independent of the magnitudes of q and $\dot{\alpha}$. The measured and smoothed yaw angular acceleration $\dot{r}$ is shown in Fig. 1b. The smoothed yaw angular acceleration $\dot{r}$ deviates from the measured values whenever the measured yaw angular acceleration exhibits "narrow peak amplitudes." The complete set of time histories have been reported in Ref. 3.

Modeling

The smoothed data from all the maneuvers were sorted and merged into a total of 50 subspaces for aerodynamic modeling. The subspaces are identified by a code (e.g., B4) as defined in Table 1, which shows the number of samples used for the modeling.

The aerodynamic parameters that were generated by the EBM algorithms are summarized in several figures. The confidence intervals of the parameters are indicated by a vertical bar (unit standard deviation). The total aerodynamic coefficient corresponding to a subspace can be computed as

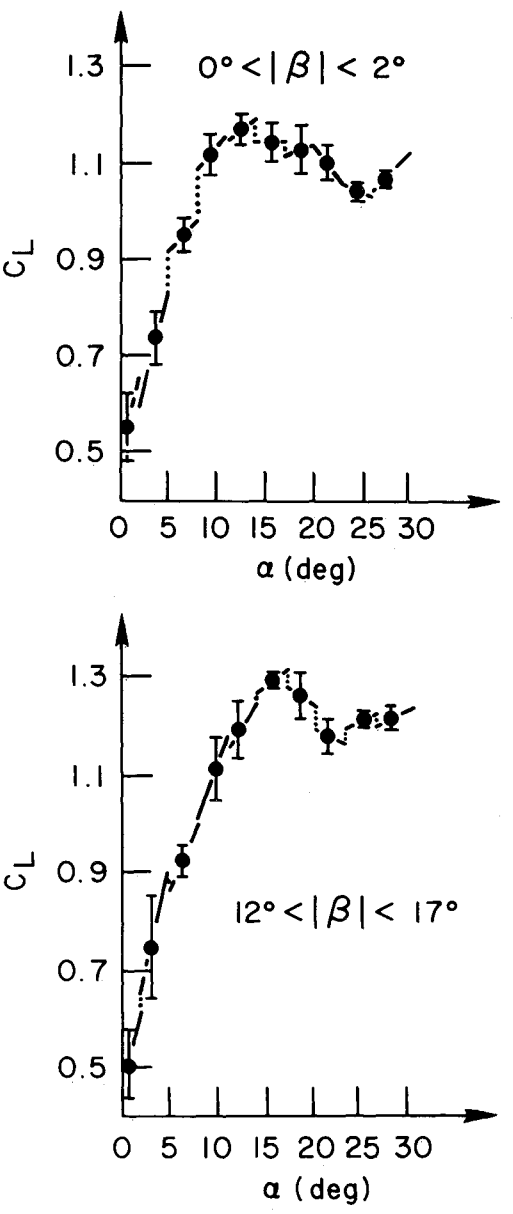

Fig. 2 Static C_L vs α.

Table 1 Number of samples in each subspace

	α deg	−2 deg	2 deg 1	5 deg 2	8 deg 3	11 deg 4	14 deg 5	17 deg 6	20 deg 7	23 deg 8	26 deg 9	30 deg 10
	0 deg	A	252	223	139	193	133	101	73	53	40	20
	2 deg	B	494	521	253	176	80	45	32	38	26	11
β	5 deg	C	257	261	89	102	66	45	56	22	29	16
d	8 deg	D	159	242	91	114	106	76	34	14	22	8
e												
g	17 deg	E	138	58	40	57	36	21	30	17	15	26

(e.g., subspace B4 is 2 deg ≤ β < 5 deg and 8 deg ≤ α < 11 deg)

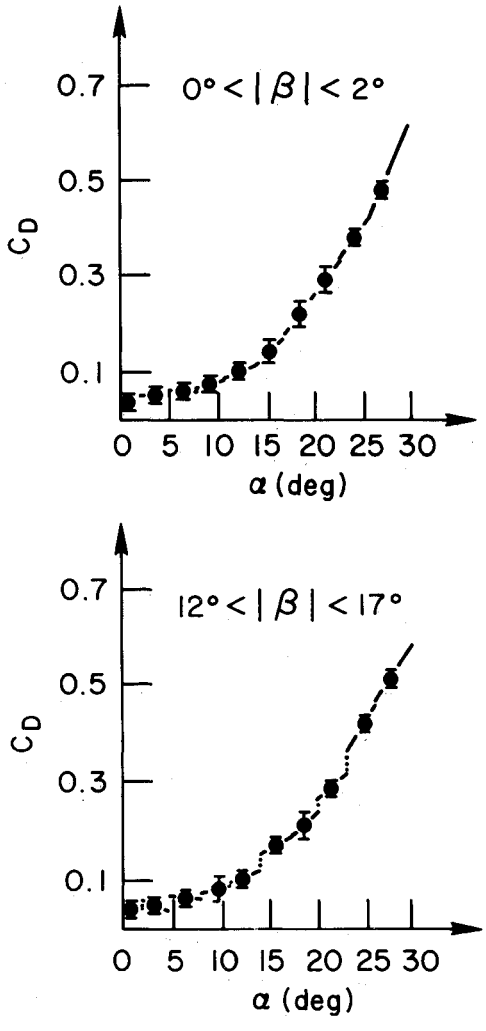

Fig. 3 Static C_D vs α.

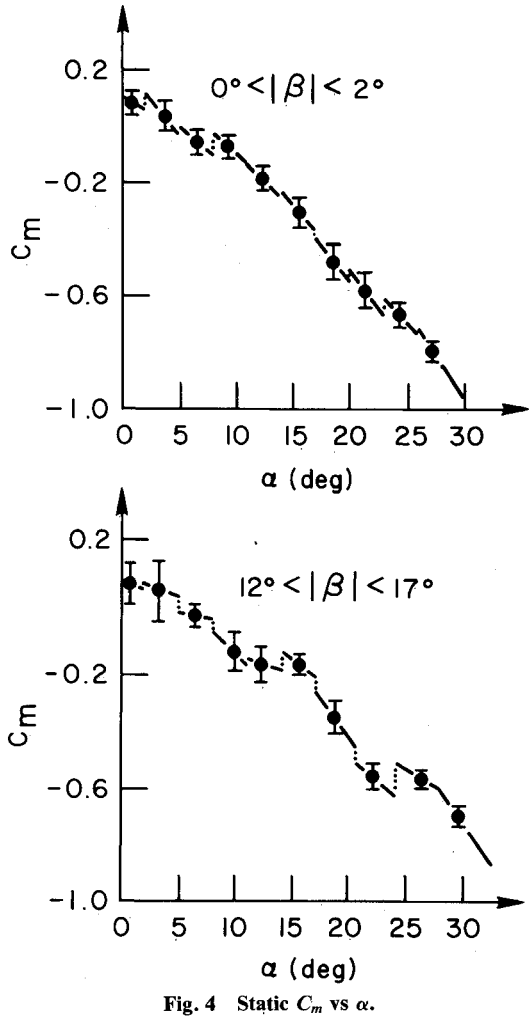

Fig. 4 Static C_m vs α.

follows:

$$C_{(\cdot)}[\alpha,\beta,\hat{p},\hat{q},\hat{r},\delta_e,\ldots] = C_{(\cdot)}[\dot{\alpha},\bar{\beta}] + C_{(\cdot)_\alpha}(-\dot{\alpha}) + C_{(\cdot)_\beta}(\beta-\bar{\beta}) + C_{(\cdot)_{\hat{p}}}\hat{p} + \ldots \quad (42)$$

where (ˆ) denotes dimensionless angular rates.[3]

Longitudinal Model

The EBM technique initially yields models for C_X, C_Z, and C_m. The customary lift (C_L) and drag (C_D) coefficients were computed using a body-to-wind axis transformation. Figure 2 shows the experimental mean lift coefficient as a function of α and β. For α below 8 deg, the lift curve is linear; beyond α = 8 deg it becomes nonlinear. The pilot observed buffeting at α = 10 deg. At about 15 deg the aircraft stalled. The mean lift coefficient shows good agreement with the corresponding slopes given by the C_{L_α} derivative. The maximum lift appears to increase with the sideslip angle. Also the angle of attack at which the maximum lift occurs increases with the sideslip angle. The loss of lift following the stall is gradual. For the purpose of referencing the figures, we define α less than 8 deg as "low α," α between 8 deg and 15 deg as "prestall," α = 15 deg as "stall," and α greater than 15 deg as "poststall" regimes.

Figure 3 shows C_D as a function of α and β. The static data in Fig. 3 show excellent transition characteristics from one subspace to the next for 0 deg ≤ β < 2 deg. At stall and beyond, the lift starts to drop; meanwhile the drag increases continuously with increasing gradient. In the stall regime, the drag increases consistently with α and β.

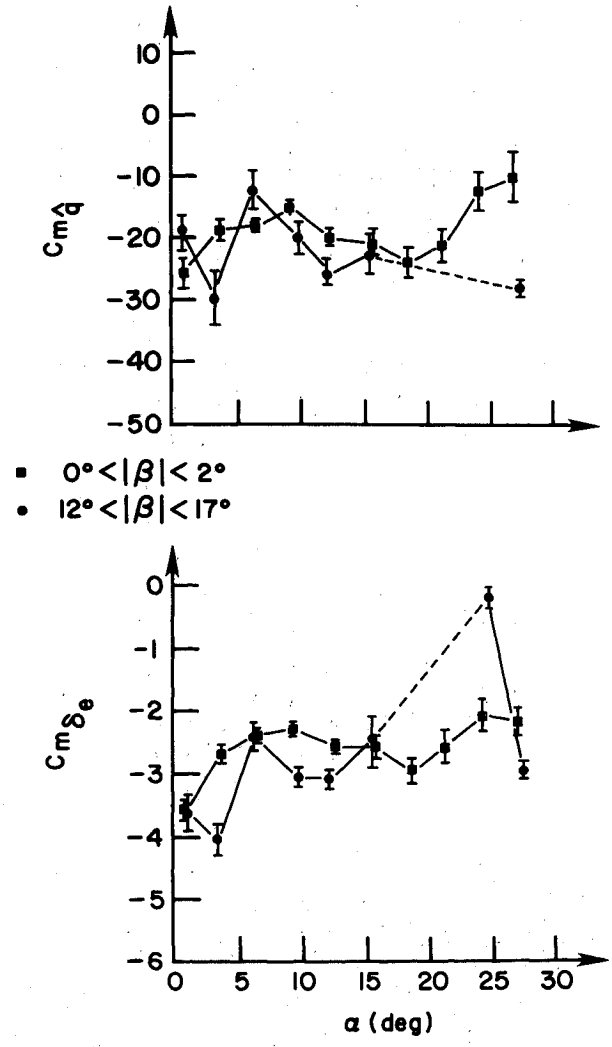

Fig. 5 Pitch moment derivatives $C_{m_{\hat{q}}}$ and $C_{m_{\delta e}}$ vs α.

Figure 4 shows the mean pitch moment coefficient C_m as a function of α and β. Stable pitch moment characteristics are obtained with no evidence of "pitch up." At high sideslip angle ($12 \leq \beta < 17$ deg), a mild pitch-up tendency is noticeable. The moments are computed with respect to the aerodynamic center. The pitch damping derivative $C_{m_{\hat{q}}}$ and pitch control derivative $C_{m_{\delta e}}$ are shown in Fig. 5. The pitch damping and pitch control power decreases gradually as α increases; at $\alpha = 18$ deg, they drop abruptly to either low values or to zero, signifying the loss of dynamic pitch stability and reduced pitch control power in the poststall region. Dashed lines are used to show the multispace trend whenever intermediate subspace(s) rendered statistically insignificant parameters. For example, in Fig. 5 when β is between 12 deg and 17 deg, the $C_{m_{\hat{q}}}$ derivative for subspaces E7, E8, and E9 is insignificant. Therefore, the subspaces E6 and E10 are connected accordingly.

Lateral-directional Model

Unlike longitudinal motion, lateral-directional motion takes place about two axes (X and Z). As a consequence, the angular rotations and control inputs not only contribute to the dynamics about their own axes but also cross couple the motion. The sideslip angle β affects the lateral-directional static force and moment coefficients much more directly than the angle of attack. Therefore, the results of the static coefficients are presented with respect to the sideslip angle.

The static side force coefficient arises principally from the fuselage and vertical tail effects, and it is shown in Fig. 6. At both low and high α, the magnitude of C_Y increases with β,

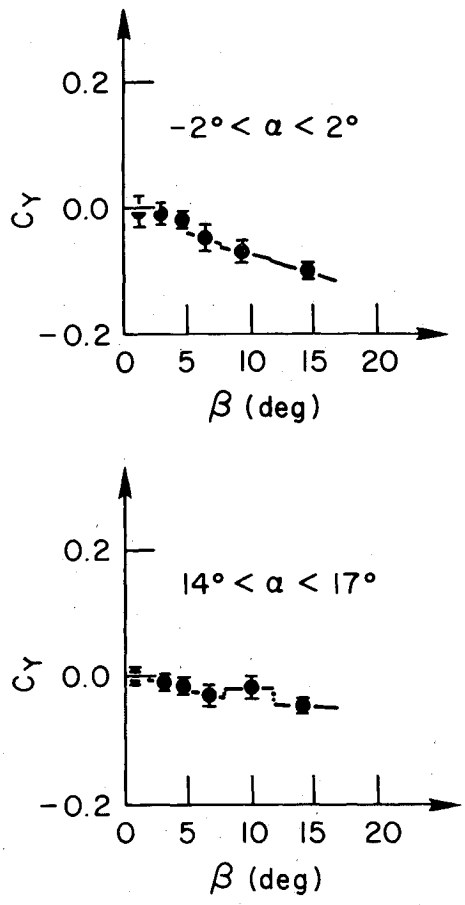

Fig. 6 Static C_Y vs β.

but at high α, the static sideforce coefficient is reduced as indicated by Fig. 6.

The wing dihedral angle (3.5 deg for the test aircraft) and aileron displacement contribute principally to the static rolling moment. The mean rolling mement coefficient is shown in Fig. 7. At low α, the sideslip angle does not contribute considerably to the C_ℓ coefficient, but it becomes strong in the poststall regime. The C_{ℓ_β} derivative at low α appears to be inconsistent with the corresponding mean values, as evident from Fig. 7. The slope is high in each subspace, but the multispace trend implies negligible slope. The reason for the anomaly should be investigated further. The "damping-in-roll" derivative $C_{\ell_{\hat{p}}}$ is crucial to the lateral stability. The negative value of $C_{\ell_{\hat{p}}}$ shown in Fig. 8 has a stabilizing effect up to stall for all β. In the poststall regime, the derivative is either positive or zero, and it can lead to "autorotation."

The yawing moment coefficient C_n is shown in Fig. 9. The mean value indicates a positive yaw mement, which helps to preserve directional stability up to stall. As the angle of attack increases, Fig. 9 shows a reduction in the effectiveness of C_{n_β}. In the poststall regime, the yaw moment begins to have a destabilizing effect. The comprehensive aerodynamic parameters have been discussed in Ref. 3.

Model Validation

The aerodynamic model extracted from the flight test data is validated using a six-degree-of-freedom numerical trajectory simulation. The simulation model starts with the measured initial condition and is driven by the measured input. The ensuing state vector time history is transformed into a measurement vector history so that it can be compared with the flight data. This approach is comprehensive; because it allows errors to propagate in time, any deficiency in one aerodynamic coefficient can cause the simulated dynamic motion to diverge. Both low-α elevator pumping and high-α

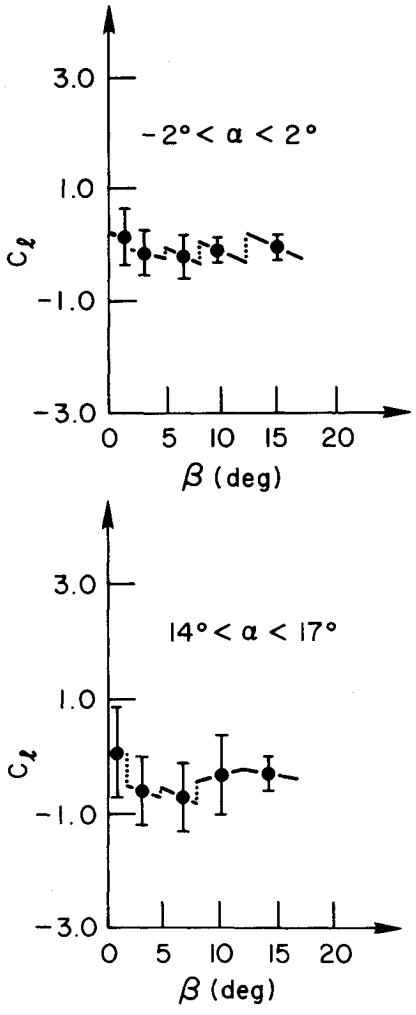

Fig. 7 Static C_l vs β.

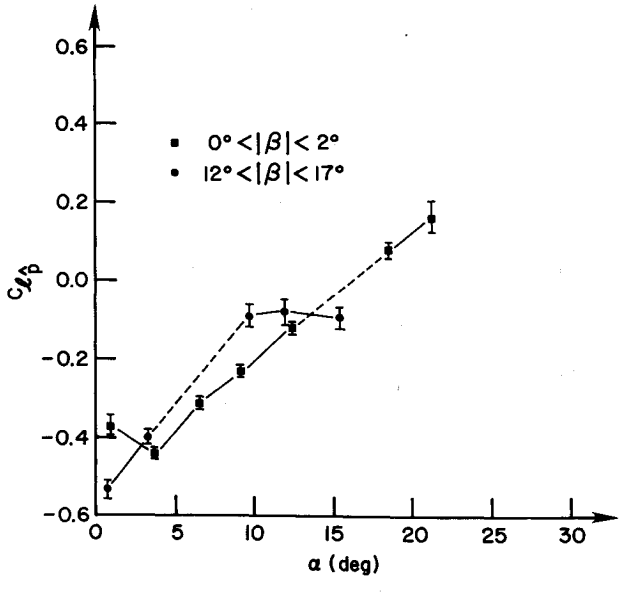

Fig. 8 Roll moment derivatives $C_{l_{\hat{p}}}$ vs α.

stall-departure maneuvers were simulated. The low-α results showed excellent match, and we present in this paper only the high-α results. Figure 10 shows the linear acceleration a_Z and pitch angular acceleration $\dot{q}$ associated with a stall maneuver. This manuever reaches a maximum pitch rate of 40 deg/s and a maximum α of 22 deg. The match is in fair agreement with the measured data.

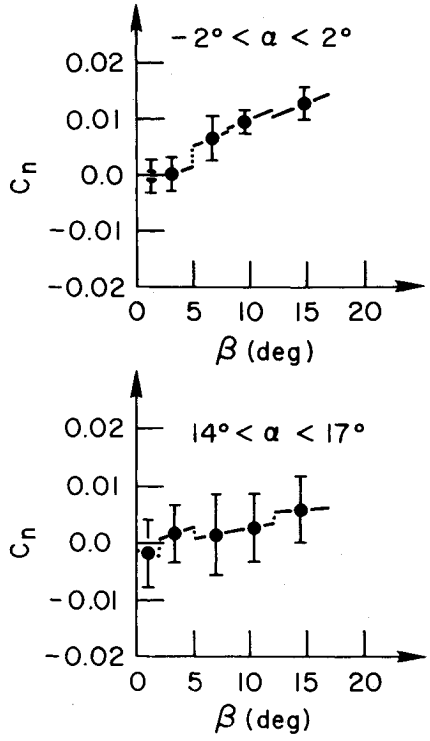

Fig. 9 Static C_n vs β.

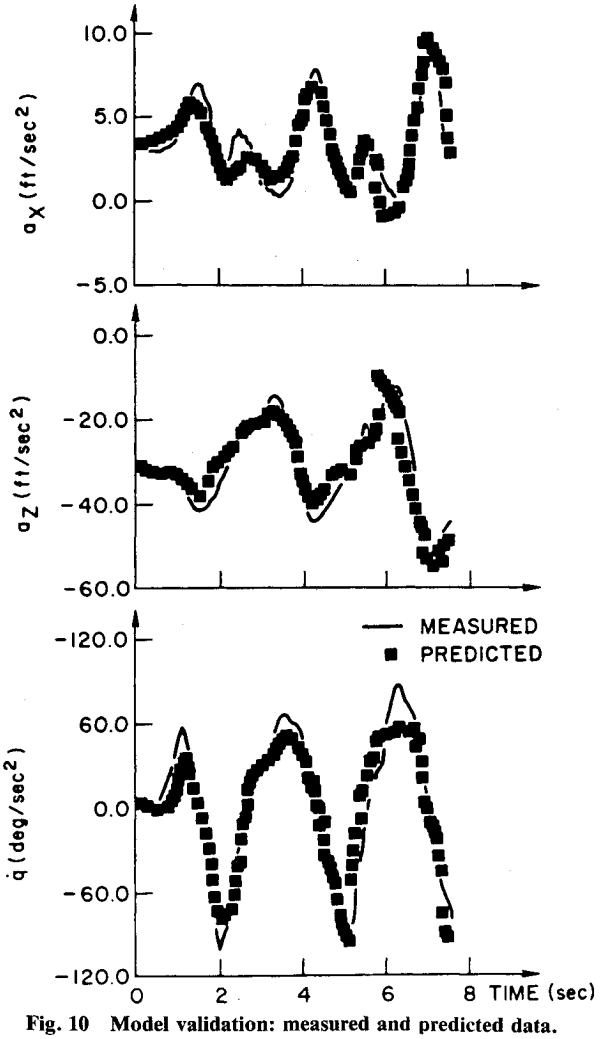

Fig. 10 Model validation: measured and predicted data.

Conclusions

The quaternion-based dynamic model is an effective tool in identification of aerodynamic coefficients, and it allows the

flight test envelope to be expanded to all-attitude maneuvers. The aircraft dynamic model augmented with the third-order Gauss-Markov process for the aerodynamic forces and moments renders a nondivering estimation algorithm. With "centering" and "orthogonalization" of independent variables, the multiple regression scheme provides satisfactory models for the aerodynamic coefficients. Employing these algorithms, the aerodynamic coefficients of the Schweizer 2-32 sailplane have been estimated from actual flight test data for angles of attack up to 30 deg and sideslip angles to ± 17 deg. The aerodynamic coefficients exhibit interesting nonlinear trends in the stall regime, many of which can be supported on theoretical grounds. It is concluded that the EBM method is capable of generating comprehensive, nonlinear, dynamic aerodynamic models from full-scale-aircraft flight test data.

Acknowledgments

This research was supported by The Schultz Foundation of Clifton, New Jersey. The Schweizer 2-32 sailplane was lent to the Flight Research Laboratory of Princeton University by the National Soaring Museum, Elmira, New York. W. B. Nixon performed flight tests. G. E. Miller provided flight test engineering support, and C. Fratter implemented the parameter estimation algorithms.

References

[1]Sri-Jayantha, M. and Stengel, R. F., "Microprocessor-based Data Acquisition System for Stall/Spin Research," *IEEE Transactions on Aerospace Electronic Systems*, Vol. AES-19, Jan. 1983, pp. 59-70.

[2]Sri-Jayantha, M. and Stengel, R.., "Data Acquisition System and Methodology for High Angle of Attack Parameter Estimation," Society of Automotive Engineers, Paper No. 830719, April 1983.

[3]Sri-Jayantha, M., "Data Acquisition and Aerodynamic Coefficient Estimation at High Angles of Attack," Princeton University Rept. No. 1624-T (Ph.D. Thesis), Princeton, NJ, Aug. 1983.

[4]Bach, R. E. and Wingrove, R. C., "Applications of State Estimation in Aircraft Flight-Data Analysis," AIAA Paper 83-2087, Aug. 1983.

[5]Iliff, K. W. and Maine, R. E., "NASA Dryden's Experience in Parameter Estimation and its Uses in Flight Test," AIAA Paper No. 82-1373, Aug. 1982.

[6]Stalford, H. L., "High-Alpha Aerodynamic Model Identification of T-2C Aircraft Using the EBM Method," *Journal of Aircraft*, Vol. 18, Oct. 1981, pp. 801-809.

[7]Fratter, C. and Stengel, R. F., "Identification of Aerodynamic Coefficients Using Flight Testing Data," AIAA Paper 83-2099, Aug. 1983.

[8]Gelb, A., *Applied Optimal Estimation*, MIT Press, Cambridge, MA, Sept. 1980, p. 188.

[9]Bierman, G. J., "Fixed Interval Smoothing with Discrete Measurements," *International Journal of Control*, Vol. 18, No. 1, 1973, pp. 65-75.

[10]Draper, N. R. and Smith, H., *Applied Regression Analysis*, 2nd Edition, John Wiley & Sons, Inc., New York, NY, 1981.

[11]Klein, V., "Identification Evaluation Methods," AGARD-LS-104, Nov. 1979, pp. 2-1 to 2-21.

[12]Sri-Jayantha, M. and Miller, G. E., "Interface Software Development for a Digital Cartridge Tape Drive," *IEEE Transactions on Instrumentation and Measurement*, Vol. IM-32, June 1983, pp. 337-342.